

On the Structure of Carbon Nanotubes: Results from Computer-Assisted Proofs

Miguel Ayala*, Rustum Choksi[†], and Benedikt Wirth[‡]

Abstract. We present a toolbox based on computer-assisted proofs to rigorously study the structure of capped carbon nanotubes. We model nanotubes as minimizers of an interatomic potential. Numerical simulations and validated computations produce rigorous mathematical results about atomic distances and structural variations. In particular, we rigorously measure the diameter, bond lengths, and bond angles of nanotubes and thereby precisely quantify oscillations near the caps, differences between interaction potentials, and effects of nanotube size or chirality. As an example, we observe that the caps induce diameter oscillations along the tube (rather than a monotonous diameter equilibration) with increasing spatial extent for less smooth interaction potentials.

Key words. Carbon Nanotubes, Molecular Mechanics, Computer-Assisted Proofs, Interatomic Potentials.

MSC codes. 65Z05, 82B05, 49S05

1. Introduction. Carbon nanotubes [9, 22, 32] are among the most remarkable structural materials known and exhibit extraordinary mechanical, electrical, and thermal properties. Their wide-ranging applications, from nanotechnology to materials science, depend critically on their geometric features, including diameter, bond angles, and chirality. Understanding how these structural attributes influence their behavior is essential for both theoretical studies and engineering applications.

One widely observed structural feature is the capping of nanotubes with half of a fullerene, another carbon allotrope. Beyond capping, variations in the chirality and geometry of the tubes introduce additional complexity, influencing the bond lengths and diameters of the tubes. A widely used method for determining these features is geometric minimization, treating nanotubes as minimizers of an energy function driven by an interaction potential that depends on atomic coordinates. Except for reduced and simplified models (reduced potentials based upon an Ansatz for the geometry as in [21, 20, 10]), proving results about the structure of local minimizers remains infeasible – the high dimensionality and complexity of widely accepted interatomic potentials make computer simulations indispensable.

On the other hand, besides the obvious difficulty of the precise interpretation of a numerical simulation, the relative variations in several geometric features of minimizers are sufficiently small that it is impossible to use simulations alone to deduce quantitative and even qualitative conclusions. A case in point is the variation of diameters, or the variations in the bond lengths, in a carbon nanotube resulting from their caps.

In this paper, we apply the theory of validated numerical computations (see [15, 38, 39, 26]). The upshot of this method is that it allows one to assert the existence of a true solution (a local minimizer) in a controlled neighborhood of the simulation. In more physical terms, it

* Department of Mathematics and Statistics, McGill University, Montréal, Canada, miguel.ayala@mail.mcgill.ca

[†]Department of Mathematics and Statistics, McGill University, Montréal, Canada, rustum.choksi@mcgill.ca

[‡]Applied Mathematics Münster, University of Münster, Münster, Germany, benedikt.wirth@uni-muenster.de

allows us to attach tiny error bars to any simulated geometric quantity for which we may assert 100 % certainty. In particular, we obtain rigorous control over the geometric structure of various carbon allotropes, including nanotubes, fullertubes [16, 35], and cyclocarbons [14], as well as evaluate the effects of different interaction potentials. For example, we obtain precise information about the different bond lengths and angles resulting from different given interaction potentials, and accurately measure the influence of the fullerene caps on the diameter variation within the carbon nanotube. Our method also the error bars to be reduced to any desired level of accuracy, constrained only by the employed computational floating point precision. A more general goal of this article is to expose and promote a toolbox for the precise analysis of general carbon allotropes and even more complicated macromolecules based upon *any* interaction potential, including those generated by machine learning algorithms ([42], [28]), when compatible with validated numerical analysis. To prove that a potential produces a certain structure, we must first understand how minimizers behave and verify that what we see in simulations is true.

The paper is organized as follows. In [section 2](#), we present our computer-assisted method for validating local minimizers of energy functions that are invariant under rotations and translations. We state a validation theorem that provides sufficient conditions for proving the existence of a local minimizer near a numerical approximation and describe how these conditions are rigorously verified computationally. In the remaining sections, we apply this method to selected nanotube geometries and interaction potentials.

In [section 3](#), we study different nanotube connectivities, including variations in chirality and cap configurations, and use computer-assisted proofs to rigorously determine geometric differences, such as variations in tube radius caused by capping, using the harmonic interatomic potential (2.2). After fixing a working level of numerical accuracy, we can also rigorously determine the duration of the oscillations in tube radius along the axis.

In [section 4](#), we analyze how different interaction potentials influence diameters, bond lengths, and angles. Using the well-known empirical Tersoff potential (4.1) [37, 36], we rigorously count the number of distinct bond lengths and bond angles in a local minimizer. We then compare this with results from a mathematically motivated potential (4.2) designed to examine the role of differentiability in the geometric properties of the tube. While we focus on specific examples for clarity of presentation, our method applies more broadly to other geometries and interaction potentials.

2. Computer-assisted Proofs for Carbon Nanotubes. We consider a system of n points in \mathbb{R}^3 , where each point represents a carbon atom. The positions of these atoms are given by

$$p_i = (x_i, y_i, z_i) \in \mathbb{R}^3, \quad i = 1, \dots, n.$$

The full set of n atoms, the atom cloud, is denoted as $p \in \mathbb{R}^{3n}$, where

$$p \stackrel{\text{def}}{=} (x_1, \dots, x_n, y_1, \dots, y_n, z_1, \dots, z_n).$$

We compute local minimizers of an energy function modeling interactions between carbon atoms. These minimizers, zeros of the energy gradient, correspond to low-energy geometries of the carbon structure. This process is often called geometry optimization. In this paper,

we focus on atomic interactions that arise solely from atomic bonding. This is particularly relevant for materials like carbon nanotubes and graphene, where bond lengths and angles play a crucial role in determining structural and electronic properties. In particular, we consider energy functions

$$(2.1) \quad E : \mathbb{R}^{3n} \rightarrow \mathbb{R}$$

that depend only on the distances between bonded atoms and the angles formed between pairs of bonds. Since rotations and translations leave distances and angles unchanged, the energy functions remain invariant under these transformations. We do not consider long-range interactions, though incorporating them into our framework would be straightforward.

A particularly simple example is to take E as the harmonic potential

$$(2.2) \quad E_h(p) \stackrel{\text{def}}{=} \sum_{ij \in B} E_b(r_{ij}) + \sum_{ij, jk \in B} E_a(\theta_{ijk}), \quad \text{with } E_b(r) = k_b(r-r_0)^2, \quad E_a(\theta) = k_\theta(\theta-\theta_0)^2,$$

with constants $k_b, k_\theta > 0$ and a preferred bond length r_0 and angle θ_0 between adjacent bonds. Here B denotes the set of atom pairs with an atomic bond, r_{ij} denotes the bond length between atoms i and j , and θ_{ijk} denotes the angle between the bonds ij and jk . Much more complicated potential energies exist and are used in the literature (such as Tersoff's potential to be introduced in (4.1)), however, the above E_h may be viewed as the second order approximation of a potential energy that includes interactions between neighboring atoms and neighboring atom pairs. Thus it is the simplest possible approximation to more complicated potentials, and the natural question arises whether this approximation exhibits any qualitatively different behavior (which we will come back to in section 4).

Finding local minimizers of E translates into a zero-finding problem for the gradient of the energy

$$F(p) \stackrel{\text{def}}{=} \nabla E(p) = 0.$$

Since the zeros of the gradient exist in a high-dimensional space, numerical simulations are essential to find and analyse these. These simulations inevitably introduce round-off and truncation errors, adding an additional level of approximation and uncertainty to our model. Our central question is: To what extent can computer simulations rigorously describe the geometry of carbon nanotubes given a potential energy function? We answer this question using computer-assisted proofs, also called rigorous numerics, which produce results at the level of mathematical proof [15, 38, 39, 26].

Suppose $\bar{p} \in \mathbb{R}^{3n}$ is an approximate solution to a zero of the gradient of some energy function E . We want to show, using a fixed-point argument, that a unique true zero of F exists within a ball centered at \bar{p} for some radius r . In particular, we will use the following result, a Newton-Kantorovich type theorem for finite-dimensional problems, which is related to the Krawczyk operator's approach [17] and the interval Newton method [23]. In the following, $\|\cdot\|$ denotes both a norm on \mathbb{R}^m as well as the induced matrix norm, while $B_r(\bar{x})$ denotes the open norm-ball around \bar{x} of radius r .

Theorem 2.1 (Validated zero). *Let $f : \mathbb{R}^m \rightarrow \mathbb{R}^m$ be differentiable and $\bar{x} \in \mathbb{R}^m$, $A \in \mathbb{R}^{m \times m}$. If for some $r^* > 0$ and $Y, Z(r^*) > 0$ we have*

$$\|Af(\bar{x})\| \leq Y, \quad \sup_{x \in B_{r^*}(\bar{x})} \|I - ADf(\bar{x})\| \leq Z(r^*),$$

then f has a unique zero in $\bar{B}_r(\bar{x})$ for any r satisfying

$$0 < r_{\min} \stackrel{\text{def}}{=} \frac{Y}{1 - Z(r^*)} \leq r \leq r^*.$$

In practice, \bar{x} will be a numerical approximation of a zero of function f , and A will be a numerical approximation to the inverse of $Df(\bar{x})$. Furthermore, we will employ the supremum norm $\|\cdot\| = \|\cdot\|_\infty$ since then the required estimates can be rigorously verified via classical interval arithmetic.

Proof. We will show that the Newton-like operator $T : \mathbb{R}^m \rightarrow \mathbb{R}^m$,

$$T(x) \stackrel{\text{def}}{=} x - Af(x),$$

has a unique fixed point in the ball $\bar{B}_r(\bar{x})$ centered at the approximate zero \bar{x} . First, we prove that T is a contraction. The condition $r_{\min} > 0$ implies $Z(r^*) < 1$. For any $x, y \in \bar{B}_r(\bar{x})$ we have

$$\|T(x) - T(y)\| \leq \sup_{z \in \bar{B}_r(\bar{x})} \|DT(z)\| \|x - y\| \leq Z(r^*) \|x - y\| < \|x - y\|.$$

Next, we show that T maps $\bar{B}_r(\bar{x})$ into itself. Let $x \in \bar{B}_r(\bar{x})$ and observe that

$$\begin{aligned} \|T(x) - \bar{x}\| &\leq \|T(x) - T(\bar{x})\| + \|T(\bar{x}) - \bar{x}\| \\ &\leq \sup_{z \in \bar{B}_r(\bar{x})} \|DT(z)\| \|x - \bar{x}\| + Y \leq Z(r^*) \|x - \bar{x}\| + Y \leq r. \end{aligned}$$

By the Contraction Mapping Theorem [6], T has a unique fixed point in $\bar{B}_r(\bar{x})$. Finally, since $Z(r^*) < 1$, the matrix A is invertible: Indeed, otherwise pick a unit norm vector v from the kernel of $ADf(\bar{x})$, then $1 = \|v\| = \|(I - ADf(\bar{x}))v\| \leq Z(r^*) \|v\| = Z(r^*) < 1$ yields a contradiction. The invertibility of A implies that f has a true zero in $\bar{B}_r(\bar{x})$. \blacksquare

The presented formulation is commonplace in the field of rigorous numerics and has been used recently for studying finite-dimensional problems, like for instance relative equilibria in the N -body problem [7, 13, 2]. We include the short proof above for completeness.

Theorem 2.1 cannot be directly applied to find zeros of ∇E since the energy E exhibits continuous invariances: Indeed, E is invariant under rotations and translations so that the zeros of ∇E form a continuous six-dimensional set, obtained by rotating or translating any critical point. **Theorem 2.1**, in contrast, provides conditions guaranteeing a unique, isolated zero within a small ball. To solve this problem, we extend the system by six additional equations that enforce orthogonality to the invariant directions near a (given, but arbitrary) numerical approximation \hat{p} of a critical point. To make the system square again, we further introduce six additional variables that act like Lagrange multipliers to the new constraints.

The extended zero-finding problem $F_{\hat{p}} : \mathbb{R}^3 \times \mathbb{R}^3 \times \mathbb{R}^{3n} \rightarrow \mathbb{R}^3 \times \mathbb{R}^3 \times \mathbb{R}^{3n}$ is given by

$$(2.3) \quad F_{\hat{p}}(\tau, \rho, p) \stackrel{\text{def}}{=} \begin{bmatrix} T_1 \cdot (\hat{p} - p) \\ T_2 \cdot (\hat{p} - p) \\ T_3 \cdot (\hat{p} - p) \\ p^T R_1 \hat{p} \\ p^T R_2 \hat{p} \\ p^T R_3 \hat{p} \\ [\nabla E(p) + S(\tau, \rho, p)] \end{bmatrix},$$

where $R_i \in \mathbb{R}^{3n \times 3n}$ for $i = 1, 2, 3$ denote the infinitesimal generators of rotations in 3D

$$R_1 = \begin{pmatrix} 0 & -I & 0 \\ I & 0 & 0 \\ 0 & 0 & 0 \end{pmatrix}, \quad R_2 = \begin{pmatrix} 0 & 0 & 0 \\ 0 & 0 & -I \\ 0 & I & 0 \end{pmatrix} \quad \text{and} \quad R_3 = \begin{pmatrix} 0 & 0 & I \\ 0 & 0 & 0 \\ -I & 0 & 0 \end{pmatrix}$$

(with $I \in \mathbb{R}^{n \times n}$ the $n \times n$ identity matrix) and $T_i \in \mathbb{R}^{3n}$ for $i = 1, 2, 3$ denote the infinitesimal generators of translations

$$[T_1]_i = \begin{cases} 1 & \text{if } 0 \leq i \leq n \\ 0 & \text{otherwise} \end{cases}, \quad [T_2]_i = \begin{cases} 1 & \text{if } n+1 \leq i \leq 2n \\ 0 & \text{otherwise} \end{cases}, \quad [T_3]_i = \begin{cases} 1 & \text{if } 2n+1 \leq i \leq 3n \\ 0 & \text{otherwise} \end{cases}.$$

Finally, function $S : \mathbb{R}^3 \times \mathbb{R}^3 \times \mathbb{R}^{3n} \rightarrow \mathbb{R}^{3n}$ is defined as

$$S(\tau, \rho, p) = \tau_1 T_1 + \tau_2 T_2 + \tau_3 T_3 + \rho_1 R_1 p + \rho_2 R_2 p + \rho_3 R_3 p.$$

The following result shows the equivalence between the zeros of $F_{\hat{p}}$ and of ∇E .

Theorem 2.2 (Removal of invariances). *Suppose $F_{\hat{p}}(\tau, \rho, p) = 0$, then also $\nabla E(p) = 0$.*

Proof. The gradient of the energy E is orthogonal to the invariant directions. That is, for each symmetry generator $i = 1, 2, 3$ it holds

$$\nabla E(p)^T R_i p = 0, \quad \nabla E(p)^T T_i = 0.$$

Hence we have

$$(2.4) \quad \nabla E(p) \cdot S(\tau, \rho, p) = \nabla E(p) \cdot (\tau_1 T_1 + \tau_2 T_2 + \tau_3 T_3 + \rho_1 R_1 p + \rho_2 R_2 p + \rho_3 R_3 p) = 0,$$

which finally implies

$$0 = [\nabla E(p) + S(\tau, \rho, p)] \cdot S(\tau, \rho, p) = S(\tau, \rho, p) \cdot S(\tau, \rho, p) = \|S(\tau, \rho, p)\|_2^2$$

and thus $S(\tau, \rho, p) = 0$. Therefore, $\nabla E(p) = 0$. ■

A similar numerical strategy appears in [11, 25] to study periodic orbits in Hamiltonian systems. In the field of computer-assisted proofs, the technique of adding variables and equations to remove continuous invariances from a zero-finding problem is also known as introducing unfolding parameters (e.g. [5]).

An immediate consequence that we will exploit in our validated numerics is the following.

Corollary 2.3 (Validated local minimizers of E). *Let $\bar{x} = (\bar{\tau}, \bar{\rho}, \bar{p}), r^*, r_{\min}, Y, Z(r^*), A$ as in [Theorem 2.1](#) for $f = F_{\hat{p}}$ and $\|\cdot\| = \|\cdot\|_{\infty}$, and abbreviate by $M_i(p) \in \mathbb{R}^{i \times i}$ the upper left submatrix of*

$$H(p) \stackrel{\text{def}}{=} \nabla^2 E(p) + T_1 T_1^\top + T_2 T_2^\top + T_3 T_3^\top + (R_1 p)(R_1 p)^\top + (R_2 p)(R_2 p)^\top + (R_3 p)(R_3 p)^\top.$$

If $(M_i^{-1}(p))_{ii} > 0$ for all $p \in B_{r_{\min}}(x)$ and $i = 1, \dots, 3n$, then E has a unique (up to continuous invariances) local minimum in $B_r(\bar{p})$ for all $r \in [r_{\min}, r^]$.*

Proof. [Theorems 2.1](#) and [2.2](#) already imply the existence of a unique critical point of E in $B_r(\bar{p})$, so it remains to show the minimizing property. To this end it suffices to show positive semi-definiteness of $\nabla^2 E(p)$ for all $p \in B_r(\bar{p})$. This in turn is implied by positive definiteness of $H(p)$, since $T_1, T_2, T_3, R_1 p, R_2 p, R_3 p$ (the invariant directions of energy E) lie in the kernel of $\nabla^2 E(p)$. By Sylvester's criterion, $H(p)$ is positive definite if and only if all its leading principal minors $\Delta_i \stackrel{\text{def}}{=} \det M_i(p)$, $i = 1, \dots, 3n$, are positive. Using the cofactor expansion for the inverse of $M_i(p)$, we have

$$M_i(p)^{-1} = \frac{1}{\Delta_i} \text{cof}(M_i(p))^\top$$

and in particular

$$\frac{\Delta_{i-1}}{\Delta_i} = [M_i(p)^{-1}]_{ii} > 0$$

for the (i, i) -entry of $M_i^{-1}(p)$. With $\Delta_0 = 1 > 0$ it follows by induction that $\Delta_i > 0$ for all i , as desired. ■

There exists several alternative methods to check the positivity of a matrix such as [\[31\]](#). Another possibility to obtain a bound for the eigenvalues is the Gershgorin circle theorem, which provides intervals enclosing the spectrum. For symmetric matrices, a more refined bound can be obtained by methods that validate each eigenvalue individually using Newton operator types arguments, as presented in [\[30\]](#).

We finally describe our computer-assisted technique, the practical application of [Corollary 2.3](#), explicitly. We begin by computing an approximate minimizer \hat{p} of E using the BFGS quasi-Newton algorithm, terminating at roughly six digits of accuracy. As initialization, for the study of capped nanotubes we simply place particles in a regular pattern on a cylindrical tube, where the exact pattern depends on the chosen nanotube chirality (see [Figure 1](#) for an example). We refine \hat{p} by applying Newton's method to the function $F_{\hat{p}}$ from [\(2.3\)](#) with initialization $(0, 0, \hat{p})$, yielding an approximate zero $\bar{x} = (\bar{\tau}, \bar{\rho}, \bar{p})$ of $F_{\hat{p}}$ with ten to twelve digits of accuracy.

To find $r^*, Y, Z(r^*)$ verifying the conditions of [Corollary 2.3](#), we use a computer in the following way. First, we compute matrix A from [Theorem 2.1](#) as the numerical inverse of $DF_{\hat{p}}(\bar{x})$. We implement the function $F_{\hat{p}}$ and its Jacobian so that they can be evaluated using intervals instead of single floating-point numbers [\[23\]](#). In other words, we employ interval arithmetic to control round-off errors. As a result, every time the computer evaluates one of our functions, the true output lies within the resulting interval, making it possible to rigorously verify inequalities. In particular, a bound Y is computed by evaluating

$$\|AF_{\hat{p}}(\bar{x})\|_{\infty}$$

in interval arithmetic (starting with our floating-point approximation \bar{x} whose entries are interpreted as intervals of vanishing width). This produces an interval that contains the true value of $\|AF_{\bar{p}}(\bar{x})\|_{\infty}$ and whose right endpoint serves as our rigorous bound Y . The rigorous bound $Z(r^*)$ for given r^* is then obtained as the right end point of the interval arithmetic output for $\|I - ADF_{\bar{p}}(X)\|_{\infty}$, in which the entries of X are intervals of radius r^* centered at the entries of \bar{x} . Observe that the ball in \mathbb{R}^n with the infinity norm is equivalent to the cartesian product of n independent intervals of radius r centered at the numerical approximation \bar{p} , it can be explicitly implemented using interval arithmetic. Finally, we compute an upper bound on r_{\min} by calculating $Y/(1 - Z(r^*))$ in interval arithmetic (treating each value as a radius-zero interval). It remains to state how r^* is chosen (the conditions in [Theorem 2.1](#) may hold for various values of r^*). In practice, we typically look for the biggest possible radius r^* such that approximately $Z(r^*) \leq \frac{1}{2}$: This leads to a large interval of uniqueness

$$(2.5) \quad \left[r_{\min} = \frac{Y}{1 - Z(r^*)}, r^* \right]$$

in [Corollary 2.3](#) (increasing r^* much further will not be possible anyway due to the condition $Z(r^*) < 1$) and at the same time a high accuracy r_{\min} of the approximated energy minimizer \bar{p} (the accuracy could at most increase twofold by making $Z(r^*)$ arbitrarily small). Such r^* is found by a bisection method.

The positivity of all $(M_i(p)^{-1})_{ii}$ for $p \in B_{r_{\min}}$ is again checked by computing $(M_i(P)^{-1})_{ii}$ in interval arithmetic for $P_j = [p_j - r_{\min}, p_j + r_{\min}]$ and validating whether the resulting interval is positive.

The code implementation and the data associated to the computer-assisted proofs in this paper are included in [\[1\]](#). All implementations use the Julia programming language. Interval arithmetic is handled with the *IntervalArithmetic.jl* Julia library [\[33\]](#). For better readability, all numbers resulting from the rigorous numerics will be given with only 5 decimal places.

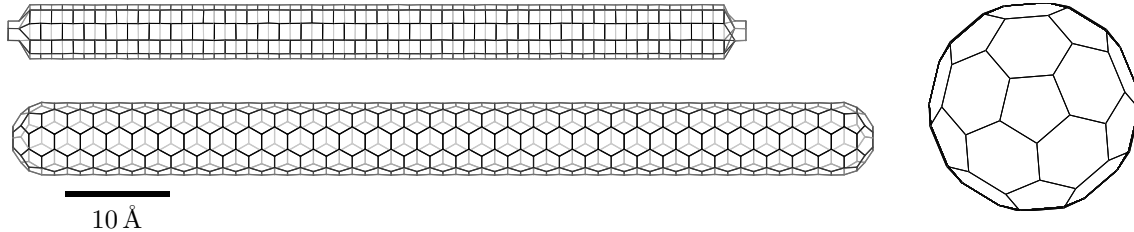


Figure 1: Top: Initialization of the BFGS gradient descent to find a local minimizer for a (5,5)-armchair nanotube using the harmonic potential E_h . Bottom and right: Validated numerical approximation of the local minimizer (side and top view).

We are now ready to explore various applications of [Corollary 2.3](#). We will consider two distinct scenarios. In [section 3](#), we fix an energy function and vary the atom connectivity to analyze structural differences between different nanotube geometries such as different chiralities or different caps. [Figure 1](#) shows a first example of a validated nanotube geometry. In [section 4](#), we instead measure the geometric effect of using different energy functions.

3. Analyzing Geometries. Matter is composed of atoms, each consisting of a nucleus of protons and neutrons surrounded by a cloud of electrons. Atoms interact by sharing electrons, forming chemical bonds that create different structures. Carbon atoms, in particular, can bond in multiple ways, leading to various structures such as graphene, fullerenes, and nanotubes.

Graphene is a two-dimensional arrangement of carbon atoms where each atom forms three sp^2 hybrid bonds with its neighbors. These bonds create a hexagonal lattice with a bond length of approximately $l = 1.42 \text{ \AA}$ and an angle of $2\pi/3$ between them. The graphene sheet can be fully described by two lattice vectors, a_1 and a_2 , both with a length of $a = l\sqrt{3}$ (see Figure 2). By rolling a graphene sheet into a cylinder, we obtain a carbon nanotube [8, 22]. The geometric classification of carbon nanotubes is based on the periodicity of this rolling process, which is given by a vector of the form

$$\mathbf{C} = na_1 + ma_2$$

with integers n, m . The resulting nanotube is said to have chirality (n, m) . Due to the hexagonal lattice symmetry, we restrict our study to chiralities of the form (n, m) with $0 < |m| < n$. Two chiralities stand out: Armchair nanotubes (n, n) have a perfectly symmetric structure along their circumference, where the carbon-carbon bonds form a continuous chain resembling the armrests of a chair. Zigzag nanotubes $(n, 0)$ feature carbon atoms aligned in straight rows along the tube's circumference, forming a repeating zigzag pattern along the edge. All other nanotubes (n, m) with $0 < |m| < n$, merely called chiral, exhibit a helical arrangement of atoms, breaking mirror symmetry and resulting in a more complex structure.

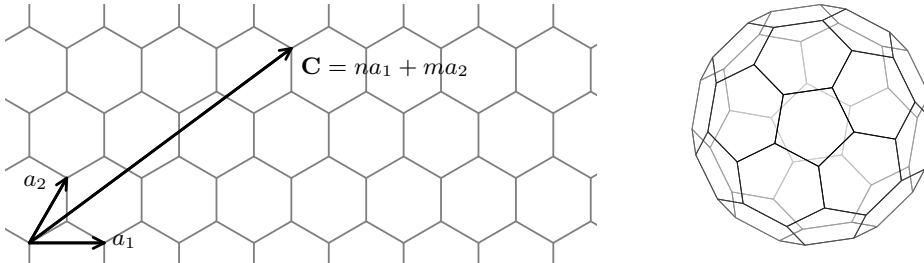


Figure 2: Left: A portion of a graphene sheet with the chiral vector $\mathbf{C} = na_1 + ma_2$ indicated. Rolling the sheet along \mathbf{C} forms a carbon nanotube with chirality (n, m) . Right: Structure of a C_{60} fullerene.

We now examine a scenario in which the energy function (2.1) remains fixed while the connectivity of the atoms is altered, modifying the geometry of the structures. In this context, we investigate the structural differences that can be rigorously observed when varying the chirality or cap configuration while employing the same interatomic potential. To this end we employ the energy E_h from (2.2) with harmonic two-atom and three-atom interaction potential, where for the modelling of carbon atoms we use the parameters $k_b = 469 \text{ kcal/mol/\AA}^2$, $r_0 = 1.44 \text{ \AA}$, $k_\theta = 63$, and $\theta_0 = 2\pi/3$, taken from [32, 41]. Let us recall again

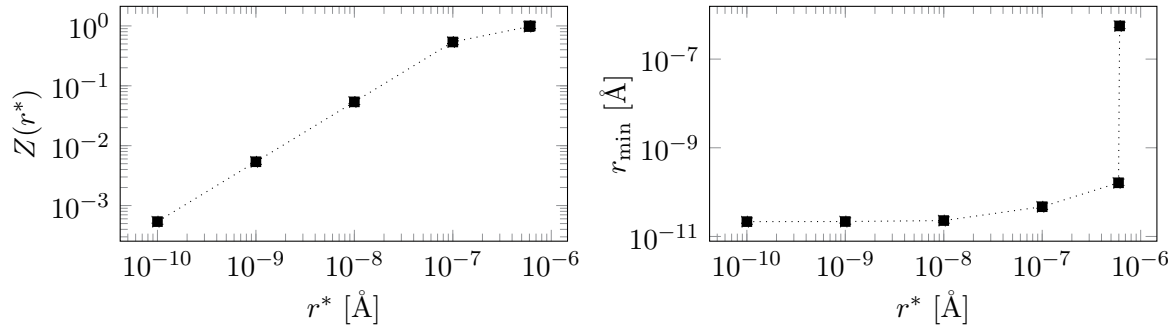


Figure 3: Dependence of $Z(r^*)$ and r_{\min} on r^* for the example of [Theorem 3.1](#).

that our approach applies to any interaction potential and the above choice represents just an example.

For our first example, we analyze the connectivity of a (5,5)-armchair nanotube with 670 atoms. This chirality allows only one fullerene cap configuration, with pentagons at the center. Each cap consists of 30 atoms, while each cross section contains 10 atoms, resulting in a total of 31 cross sections. We sometimes refer to cross sections as *rings*. Once we select the connectivity to analyze, the first step is to approximate the solution.

[Figure 1](#) shows a numerical approximation of a local minimizer of the energy function (2.2) for a (5,5)-armchair nanotube with caps, which provably lies within a $5 \cdot 10^{-11}$ Å distance from the true local minimizer.

Theorem 3.1 (Capped armchair nanotube). *Consider the approximate local minimizer $\bar{p} \in \mathbb{R}^{3n}$ of E_h from (2.2) (with bonds corresponding to the (5,5)-armchair capped nanotube with $n = 670$) shown in [Figure 1](#). A true local minimizer of E_h lies within distance $4.6844 \cdot 10^{-11}$ Å of \bar{p} and is unique within distance $9.9993 \cdot 10^{-8}$ Å of \bar{p} (in the norm $\|\cdot\|_\infty$).*

Proof. This is merely an application of [Corollary 2.3](#) with numerically found \bar{p} as well as $\bar{\tau}, \bar{\rho}, A$ and all conditions rigorously verified numerically via interval arithmetic for the values $r^* = 9.9993 \cdot 10^{-8}$ Å, $Z(r^*) = 5.3880 \cdot 10^{-1}$, and $Y = 2.1601 \cdot 10^{-11}$ Å, resulting in $r_{\min} = Y/(1 - Z(r^*)) \leq 4.6844 \cdot 10^{-11}$ Å. The detailed computational procedure was already described after [Corollary 2.3](#). [Figure 3](#) illustrates the numerical dependence of $Z(r^*)$ and r_{\min} on the choice of r^* (recall that we choose r^* so that $Z(r^*) \approx 1/2$). It shows that, employing different choices of r^* , one can even improve the accuracy estimate r_{\min} for the approximate minimizer by a factor 2 and increase the uniqueness radius r^* by a factor of roughly 6. ■

What can we learn from results like [Theorem 3.1](#)? We begin by examining the impact of the caps on the nanotube’s radius. To this end we first align the computed nanotube’s axis with the z -axis and compute the distance from each atom to the z -axis. Together with [Theorem 3.1](#) this produces an interval for each atom, which we represent as error bars in our plots. The intervals are small enough that any visible distinctions in the plot are mathematically rigorous—*what we see is what we can prove*.

Remark 3.2 (The radius of the nanotube). Carbon nanotube structures are not perfect

cylinders, but polyhedral. When we refer to the *radius of the tube*, we mean the distance from an atom to the axis of the tube. The radius of the of an ideal (n, m) nanotube-cylinder of bond length r_0 is given by [4]

$$\frac{r_0}{2\pi} \sqrt{3(n^2 + m^2 + nm)}.$$

Since bond lengths in carbon nanotubes slightly deviate from those in planar graphene, we adopt a bond length of $r_0 = 1.44 \text{ \AA}$ [32]. For the $(5,5)$ armchair nanotube this results in a radius of 3.4377 \AA .

We present our results in Figure 4. The horizontal axis indicates the index of each cross section, with zero corresponding to the middle of the tube. The vertical axis, shown on a logarithmic scale, displays the difference between each atom's distance to the nanotube axis and the average distance in the middle cross section, excluding atoms in the caps. Each visible dot corresponds to ten overlapping error bars (one per each atom of the cross section), showing the interval within which the deviation lies for the true energy minimizer.

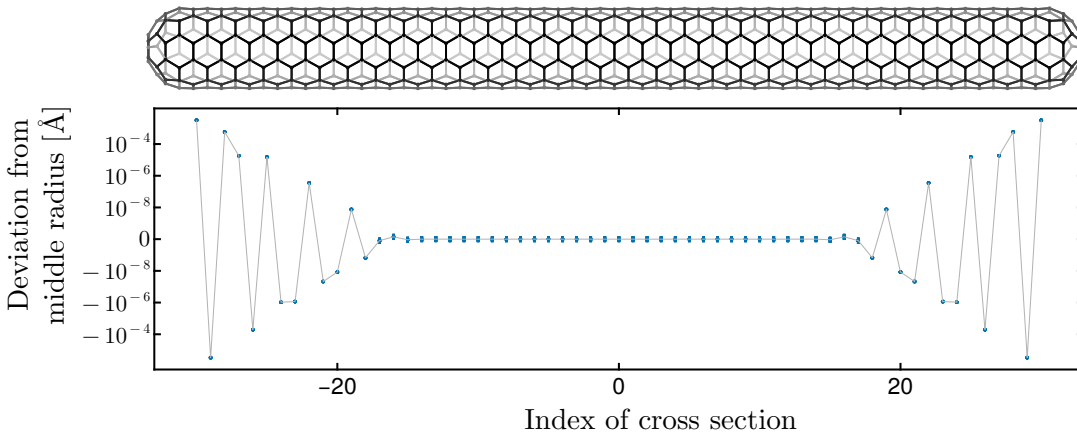


Figure 4: A $(5,5)$ -armchair nanotube configuration with 670 atoms for the harmonic potential E_h proven to be energy minimizing with computer assistance. The plot underneath is aligned with the nanotube and shows the deviation of the distance between each atom and the nanotube axis from the mean distance in cross section 0. Each dot represents ten overlapping error bars (too small to be resolved in the figure), one for each atom of the cross section.

For example, the slight misfit between the native cap and nanotube diameter provably leads to oscillations in the nanotube diameter, shown in Figure 4. The amplitude of these oscillations decreases exponentially away from the caps until at cross section ± 17 it reaches a size that can no longer be resolved by the numerical accuracy of our proof (but would be resolved when working with higher numerical precision). Figure 5 zooms in on cross sections -17 to 17 so that the error bars become visible. As can be seen, the diameters of these cross sections (distance between opposite atoms) provably coincide up to 10 digits of accuracy, taking the value of 6.949375982 \AA . As expected from the exponential decay of the cap

influence, also a shorter nanotube shows the exact same behavior, see [Figure 6](#). This does not change either for a nanotube with an even number of cross sections as shown in [Figure 7](#) (only tube configuration shown), where the reflection symmetry across the nanotube's midplane is lost (the central pentagon of one cap is rotated relative to the other).

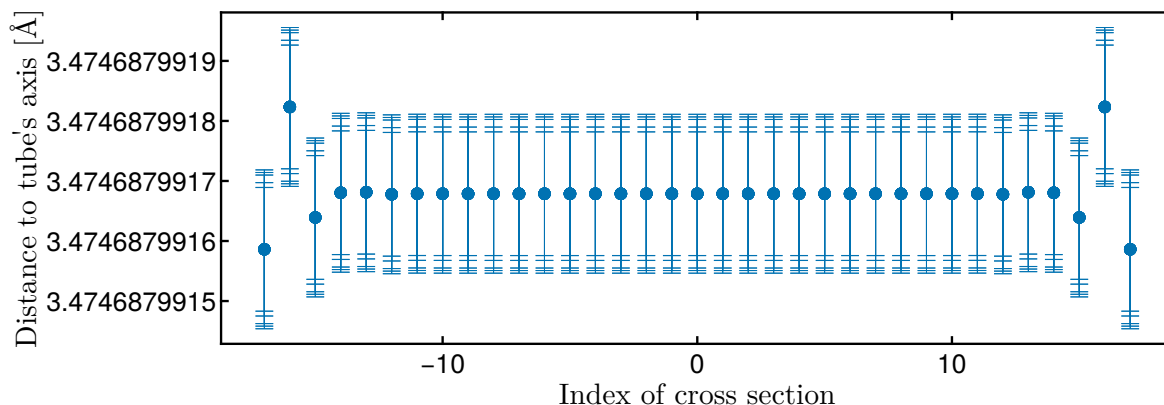


Figure 5: A zoom-in of the middle section of the plot in [Figure 4](#). The ten overlapping error intervals are now visible. The dots represent their midpoints. In this section of the tube, the computer-assisted proof, with the current accuracy, does not allow to detect oscillations in the radius.

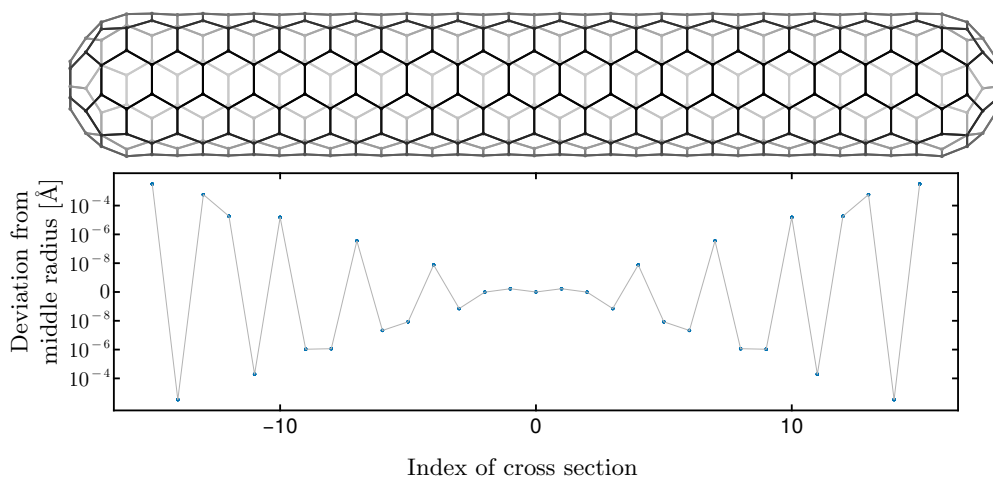


Figure 6: Same as [Figure 4](#) for a (provably energy-minimizing) (5,5)-armchair nanotube with 370 atoms.

Let us now focus our analysis on a different geometry: the (10,0)-zigzag nanotube with caps consisting of 660 atoms. This chirality features cross sections composed of ten atoms, similar to the (5,5)-armchair nanotube previously presented. We first rigorously validate the

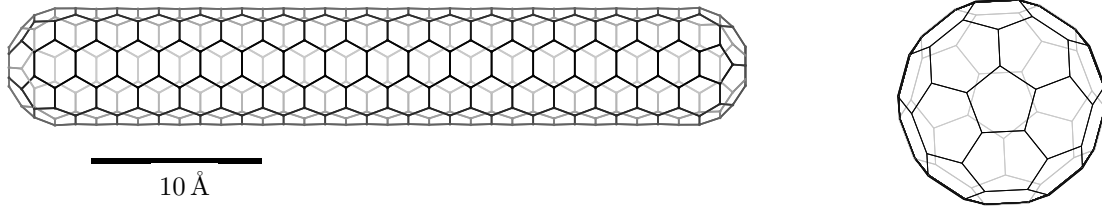


Figure 7: A numerically validated approximation of a local energy minimizer for a capped (5,5)-armchair nanotube with an even number of cross sections, using the harmonic potential E_h . In this case, the reflection symmetry is lost (compare Figure 1).

numerical approximation shown in Figure 8. The proof is analogous to the one of Theorem 3.1.

Theorem 3.3 (Capped zigzag nanotube). *Consider the approximate local minimizer $\bar{p} \in \mathbb{R}^{3n}$ of E_h from (2.2) (with bonds corresponding to the (10,0)-zigzag capped nanotube with $n = 660$) shown in Figure 8. A true local minimizer of E_h lies within distance $1.2226 \cdot 10^{-11}$ Å of \bar{p} and is unique within distance $9.9902 \cdot 10^{-8}$ Å of \bar{p} (in the norm $\|\cdot\|_\infty$).*

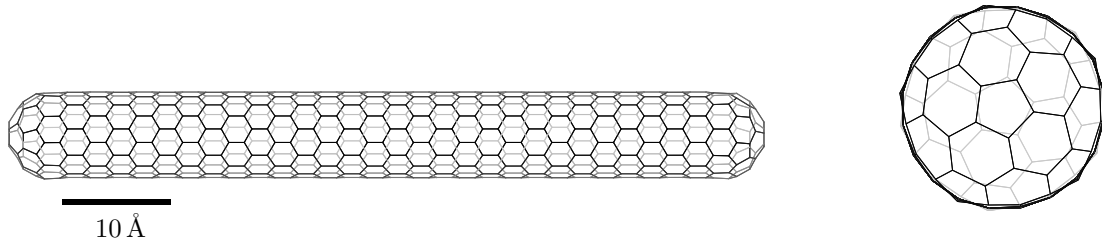


Figure 8: A numerically validated approximation of a local energy minimizer for a (10,0)-zigzag nanotube with pentagonally symmetric caps, using the harmonic potential E_h .

Just like for the (5,5)-armchair nanotube, the diameters of the cross-sections oscillate with amplitude exponentially decreasing away from the caps, but the type of oscillations is qualitatively different as illustrated in Figure 9: Every third and fourth cross section has perfect diameter (the same as the middle cross sections), while for every other cross section half the atoms has a larger and the other half a smaller distance from the nanotube axis (where the deviation to larger and smaller distances is symmetric).

The (10,0)-zigzag nanotube can be fitted with an alternative cap that has a hexagon at its center and dihedral D_2 -symmetry [18]. Figure 10 shows a numerical approximation of the (10,0)-zigzag nanotube with these caps. This numerical approximation is validated analogously to Theorems 3.1 and 3.3. To illustrate another application of our method, we provide rigorous measurements of the energy. As with all other numerical quantities, the energy evaluation produces a thin interval containing the true value, so we report the validated digits (those that stay the same over the full interval). Table 1 lists the rigorous energy per atom for the five tube geometries presented. As expected, one observes that the energy per

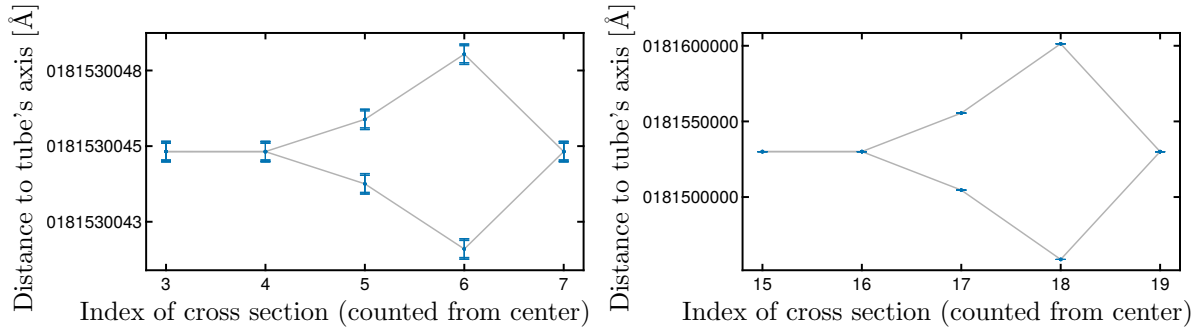


Figure 9: Distance of each atom to the nanotube axis for the (10,0)-zigzag validated nanotube from [Theorem 3.3](#).

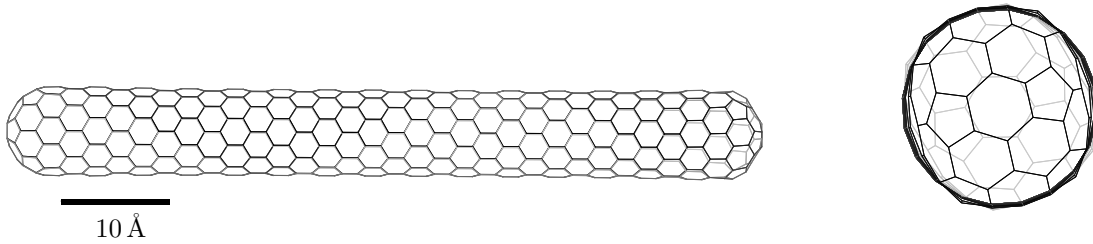


Figure 10: A numerically validated approximation of a local energy minimizer for a (10,0)-zigzag nanotube with D_2 -symmetric caps, using the harmonic potential E_h .

atom decreases with increasing atom number since the influence of the caps decreases. We also see that the (10,0)-zigzag nanotube is energetically more favorable than the (5,5)-armchair nanotube.

Chirality	Cap symmetry	Atoms	Energy per atom
(5,5)	Pentagonal	670	0.31100507
(5,5)	Pentagonal	370	0.50733624
(5,5)	Pentagonal	360	0.51951604
(10,0)	Pentagonal	660	0.28820774
(10,0)	D_2	364	0.29632260

Table 1: Energy per atom for different chiralities using the harmonic potential.

Besides other tube chiralities, we can analyze additional carbon structures, such as fullerenes and cyclocarbons [16, 35, 14]. We can also incorporate periodic offset conditions to model an infinite tube. In this setting, the nanotube is represented as a structure of atoms with boundary conditions, where atoms on the bottom boundary interact with those on the top. The key difference is that these periodic boundary conditions remove one rotational

symmetry so that the validation map (2.3) needs to be modified.

In the next section, we consider the case of fixed atomic connectivity and show how computer-assisted proofs can be used as a tool for the rigorous analysis of an interaction potential.

4. Analyzing Interaction Potentials. Interactions between carbon atoms are governed by quantum mechanical principles. A full description from first principles requires modeling the motion of both nuclei and electrons. However, because nuclei are much heavier than electrons, we can treat their motion independently. This simplification is known as the *adiabatic approximation*.

A further simplification, the *Born–Oppenheimer approximation*, assumes that the potential energy governing nuclear motion equals the electronic potential energy. For intuition, we can think as follows: a pair of atoms forms a bond by sharing electrons. In this sense, electrons act as a glue holding the nuclei together. The electronic potential energy corresponds to the elastic energy of this electronic glue—the *interaction potential*. Quantum mechanical calculations of this energy have been carried out with high precision. For a pair of atoms, the energy reaches a minimum at a specific interatomic distance. It rises steeply at short distances and gradually approaches a constant as the nuclei separate.

To simplify its study, one often uses analytical approximations of the electronic potential energy such as the harmonic potentials used in Section 3. This idea extends to larger systems, where the potential energy depends on all atomic coordinates. These models determine the interatomic forces and thus the geometry of the structure. For more details on these approximations and the derivation of effective potentials, an accessible reference are the books [12, 40].

Remark 4.1. The harmonic potential used in (2.2) can be seen as a second-order approximation of the Morse potential [24] near its minimum.

More general forms of energy have been used to model interaction energies, for example the bond order potentials [37, 3, 27] such as Tersoff’s potential

$$(4.1) \quad E_T(p) \stackrel{\text{def}}{=} \frac{1}{2} \sum_{i \neq j} f_C(r_{ij}) \left[A e^{-\lambda_1 r_{ij}} - b_{ij} B e^{-\lambda_2 r_{ij}} \right],$$

where the indices i and j run over the atoms of the system and r_{ij} denotes the distance between atoms i and j . The cutoff function is defined as

$$f_C(r) = \begin{cases} 1, & r < R - D, \\ \frac{1}{2} \left\{ 1 - \sin \left[\frac{\pi(r-R)}{2D} \right] \right\}, & R - D < r < R + D, \\ 0, & r > R + D, \end{cases}$$

with R chosen so that only the first-neighbor shell of atoms is included for most structures of interest. The bond order function is given by

$$b_{ij} = \left(1 + \beta^n \zeta_{ij}^n \right)^{-\frac{1}{2n}} \quad \text{with} \quad \zeta_{ij} = \sum_{k \neq i, j} f_C(r_{ik}) g(\theta_{ijk}),$$

where θ_{ijk} is the angle between bonds $i-j$ and $i-k$. The angular function is defined as

$$g(\theta) = 1 + \frac{c^2}{d^2} - \frac{c^2}{d^2 + (h - \cos \theta)^2}.$$

The model parameters listed in Table 2 stem from [36], alternative values are found in [19].

A	1393.6 eV	β	1.5724×10^{-7}	h	-0.57058
B	346.74 eV	n	0.72751	R	1.95 Å
λ_1	3.4879 Å	c	38049	D	0.15 Å
λ_2	2.2119 Å	d	4.3484		

Table 2: Tersoff potential parameter values for carbon taken from [36].

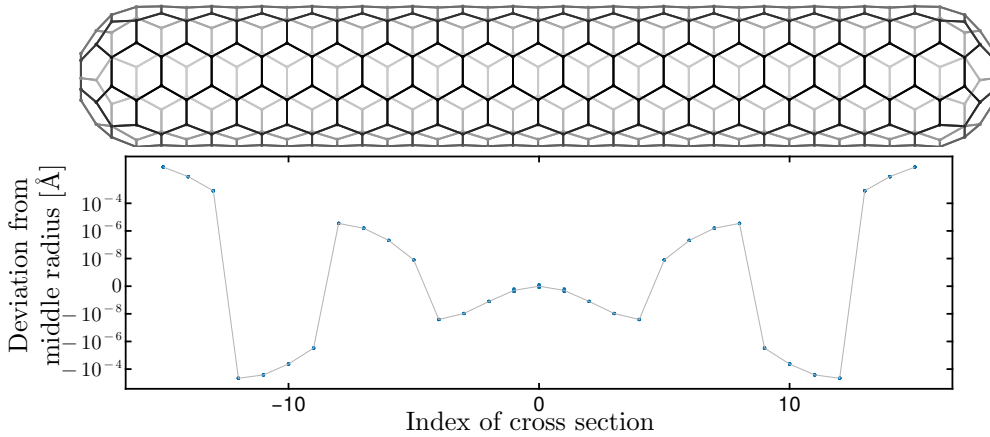


Figure 11: Same as Figure 6, only replacing the harmonic potential (2.2) by the Tersoff potential (4.1).

A potential of this type, with many parameters and composed functions, added to the high dimension of the problem, requires the use of a computer for its analysis. A computer-assisted proof approach as the one we are presenting can be used to draw rigorous conclusions about local minimizers of the energy function using a numerical simulation. The implementation of such a validation theorem can be simplified by computing the Hessian matrix of the energy via automatic differentiation. Libraries for interval arithmetic, such as *IntervalArithmetic.jl* in Julia [33] and *INTLAB* in MATLAB [29], support rigorous derivative computation through forward-mode differentiation [38]. This is particularly useful for potential applications involving modern interatomic potentials—such as those obtained from machine learning methods ([42], [28])—that are only available as numerical functions. In such cases, the applicability of our method depends on compatibility with interval arithmetic, as the structure of the numerical potential may lead to significant overestimations in the resulting interval enclosures.

We use Corollary 2.3 to validate numerical simulations using Tersoff's potential E_T with the original set of parameters from [36].

Theorem 4.2 (Capped armchair nanotube with Tersoff potential). *Consider the approximate local minimizer $\bar{p} \in \mathbb{R}^{3n}$ of E_T from (4.1) (with bonds corresponding to the (5,5)-armchair capped nanotube with $n = 370$) shown in Figure 11. A true local minimizer of E_T lies within distance $4.6110 \cdot 10^{-11}$ Å of \bar{p} and is unique within distance $9.9212 \cdot 10^{-8}$ Å of \bar{p} (in the norm $\|\cdot\|_\infty$).*

As in the previous section we start by examining oscillations in the tube radius. Figure 11 shows that for the Tersoff potential, just like for the harmonic potential (compare Figure 6), the atom distance from the tube axis oscillates around a value with amplitude decaying exponentially fast away from the caps. The magnitude of the oscillation is comparable to the harmonic potential, but the structure is different with groups of four consecutive cross-sections having either a larger or a smaller distance. The central tube radius is 3.53221 Å.

Another qualitative difference between energy minimizers of the Tersoff energy (4.1) and the harmonic energy (2.2) is that the Tersoff energy minimizer exhibits *multiple different* lengths of interatomic bonds. In particular, as Figure 12 shows, there are two preferred bond length values: The bond lengths within each cross section (1.4759 Å) differ from those between two cross-sections (1.4707 Å). We also observe two distinct bond angles, 2.07296 and 2.08030 (which both are smaller than $2\pi/3$). The smaller angle is adjacent to the bonds within a cross-section while the larger one occurs everywhere else.

The Tersoff potential is an example of a parameterized function whose parameters are fit to measurement data. The choice of ansatz functions can here lead to qualitative differences. As our final example, we thus consider the following non-physical Huber-norm potential

$$(4.2) \quad E_H^\epsilon(p) \stackrel{\text{def}}{=} \sum_{ij \in B} \sqrt{(1 - r_{ij}/r_0)^2 + \epsilon} \quad + \quad \sum_{ij, jk \in B} \sqrt{(\frac{2\pi}{3} - \theta_{ijk})^2 + \epsilon},$$

which features a more pronounced minimum. The parameter ϵ essentially controls the level of smoothness (as $\sqrt{a^2 + \epsilon}$ tends to $|a|$ for $\epsilon \rightarrow 0$). Figure 13 shows a numerically computed (5,5)-armchair nanotube with $n = 670$ atoms. It identifies oscillations in the cross-sectional radii that sustain to a much larger distance from the caps than for the harmonic or the Tersoff potential. Again, the natural question raised by this observation is whether these oscillations are genuine features of the system or instead artifacts of the numerical computation? And again, this can be answered by rigorous validation, where with this final example we also highlight that the validation method can use and may in some cases require higher numerical precision: For simulations based on the energy function (4.2), we use quadruple precision to compute the numerical approximation and octuple precision for the validation step using Corollary 2.3.

Theorem 4.3 (Capped armchair nanotube with Huber potential). *Consider the approximate local minimizer $\bar{p} \in \mathbb{R}^{3n}$ of E_H from (4.2) for $\epsilon = 10^{-5}$ (with bonds corresponding to the (5,5)-armchair capped nanotube with $n = 670$) shown in Figure 13. A true local minimizer of E_H lies within distance $1.8805 \cdot 10^{-37}$ Å of \bar{p} and is unique within distance $8.1854 \cdot 10^{-14}$ Å of \bar{p} (in the norm $\|\cdot\|_\infty$).*

Remark 4.4 (Nonsmooth potential). Realistic physical potentials should not exhibit singularities such as discontinuities or nondifferentiabilities (*natura non facit saltus*), which is why

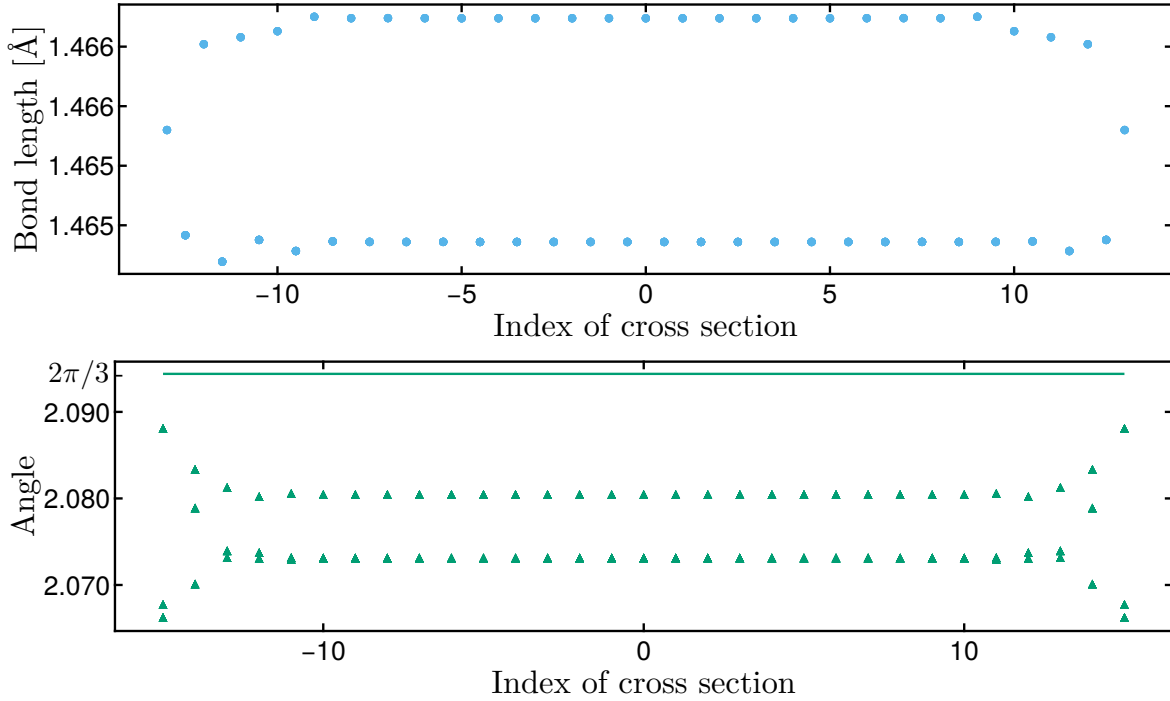


Figure 12: Bond lengths (top) and bond angles (bottom) of the numerically validated approximation from Figure 11 of a local energy minimizer for a capped (5, 5)-armchair nanotube with 370 atoms, using the Tersoff potential. Markers at noninteger indices correspond to bonds between two cross-sections.

we employed rigorous numerical techniques that apply to differentiable energies. However, it is conceivable that physical potentials can have different degrees of smoothness such as more or less pronounced minima, which we emulate by varying parameter ϵ in (4.2). This does indeed have a qualitative influence on the geometry of the nanotube: While with increasing distance from the caps the nanotube radius quickly reaches a constant equilibrium value for the harmonic and the Tersoff potential, this does not happen for the less smooth potential with small ϵ (see Figure 13); the smaller ϵ , the longer-lived are the oscillations. In fact, in the limit $\epsilon \rightarrow 0$ it is expected that the radii of the transversal atom rings oscillate at a fixed amplitude along the full length of the capped nanotube. Indeed, under the simplifying assumptions of fixed prescribed bond lengths and dihedral D_5 -symmetry (properties that are exhibited anyway by our rigorously found nanotube configurations), such a behavior was shown in [34, Thm. 3] for infinitely long armchair-(5,5)-nanotubes that contain an atom ring with perturbed radius.

Acknowledgments. BW and RC were supported by the Deutsche Forschungsgemeinschaft (DFG, German Research Foundation) under Germany’s Excellence Strategy EXC 2044-390685587, Mathematics Münster: Dynamics-Geometry-Structure. BW further gratefully acknowledges support by the DFG, priority program SPP 2256, Grant WI 4654/2-2, and by the

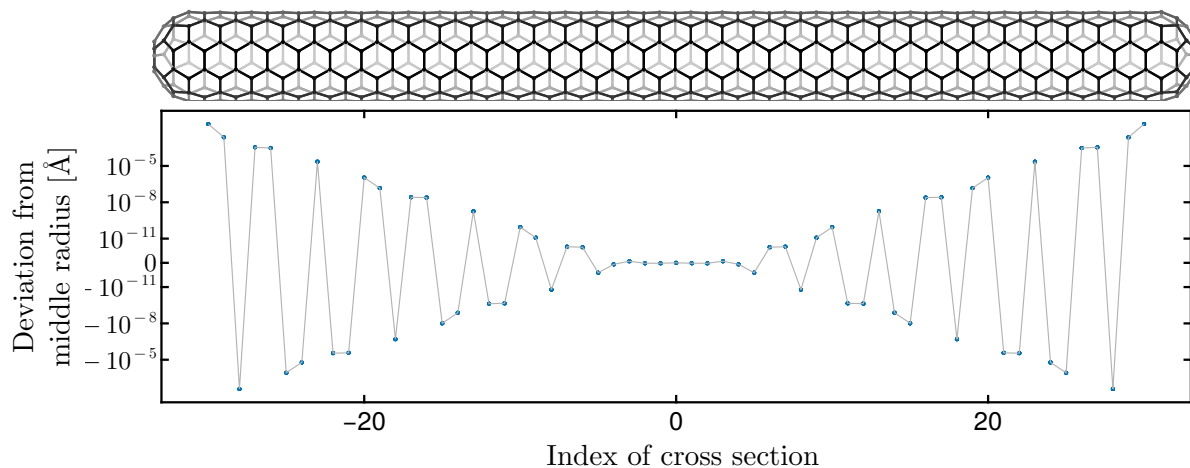


Figure 13: Same as Figure 4, only replacing the harmonic potential (2.2) by the Huber-type potential (4.2) with $\epsilon = 10^{-5}$.

Department of Mathematics and Statistics at McGill University. RC acknowledges support of NSERC (Canada) via its Discovery Grants Program and the support of the University of Münster as a Münster Research Fellow. MA and RC thank Jean-Philippe Lessard for several helpful discussions.

REFERENCES

- [1] M. AYALA, *Codes for on the structure of carbon nanotubes: Results from computer-assisted proofs*. <https://github.com/mi-ayala/NanotubesCAPs>, 2025.
- [2] I. BALÁZS, J. B. VAN DEN BERG, J. COURTOIS, J. DUDÁS, J.-P. LESSARD, A. VÖRÖS-KISS, J. F. WILLIAMS, AND X. Y. YIN, *Computer-assisted proofs for radially symmetric solutions of pdes*, *Journal of Computational Dynamics*, 5 (2018), pp. 61–80.
- [3] D. W. BRENNER, *Empirical potential for hydrocarbons for use in simulating the chemical vapor deposition of diamond films*, *Physical Review B*, 42 (1990), pp. 9458–9471, <https://doi.org/10.1103/PhysRevB.42.9458>.
- [4] M. BUDYKA, T. ZYUBINA, A. RYABENKO, S. LIN, AND A. MEBEL, *Bond lengths and diameters of armchair single wall carbon nanotubes*, *Chemical Physics Letters*, 407 (2005), pp. 266–271, <https://doi.org/https://doi.org/10.1016/j.cplett.2005.03.088>, <https://www.sciencedirect.com/science/article/pii/S0009261405004252>.
- [5] R. CALLEJA, C. GARCÍA-AZPEITIA, O. HÉNOT, J.-P. LESSARD, AND J. D. M. JAMES, *From the lagrange triangle to the figure eight choreography: Proof of marchal’s conjecture*, 2024, <https://arxiv.org/abs/2406.17564>, <https://arxiv.org/abs/2406.17564>.
- [6] C. CHICONE, *Ordinary Differential Equations with Applications*, vol. 34 of Texts in Applied Mathematics, Springer, New York, 2nd ed., 2006.
- [7] K. CONSTANTINEAU, C. GARCÍA-AZPEITIA, AND J.-P. LESSARD, *Spatial relative equilibria and periodic solutions of the coulomb (n+1)-body problem*, *Qualitative Theory of Dynamical Systems*, 21 (2022), pp. Paper No. 3, 19.
- [8] M. DRESSELHAUS, G. DRESSELHAUS, AND R. SAITO, *Physics of carbon nanotubes*, *Carbon*, 33 (1995), pp. 883–891, [https://doi.org/https://doi.org/10.1016/0008-6223\(95\)00017-8](https://doi.org/https://doi.org/10.1016/0008-6223(95)00017-8), <https://www.sciencedirect.com/science/article/pii/0008622395000178>. Nanotubes.

- [9] M. S. DRESSELHAUS, G. DRESSELHAUS, AND P. AVOURIS, eds., *Carbon Nanotubes: Synthesis, Structure, Properties, and Applications*, vol. 80 of Topics in Applied Physics, Springer, 2001, <https://doi.org/10.1007/3-540-39947-X>.
- [10] M. FRIEDRICH, E. MAININI, P. PIOVANO, AND U. STEFANELLI, *Characterization of optimal carbon nanotubes under stretching and validation of the cauchy–born rule*, *Archive for Rational Mechanics and Analysis*, 231 (2019), pp. 465–517, <https://doi.org/10.1007/s00205-018-1284-7>, <https://doi.org/10.1007/s00205-018-1284-7>.
- [11] C. GARCÍA-AZPEITIA, W. KRAWCEWICZ, M. TEJADA-WRIEDT, AND H. WU, *Global nonlinear normal modes in the fullerene molecule C_{60}* , *SIAM Journal on Applied Dynamical Systems*, 20 (2021), pp. 94–129, <https://doi.org/10.1137/19M1269865>, <https://doi.org/10.1137/19M1269865>.
- [12] B. GELIN, *Molecular Modeling of Polymer Structures and Properties*, Hanser Publishers, 1994, <https://books.google.ca/books?id=R350QgAACAAJ>.
- [13] O. HÉNOT AND C. ROUSSEAU, *Spiderweb central configurations*, *Qualitative Theory of Dynamical Systems*, 18 (2019), pp. 1135–1160.
- [14] K. KAISER, L. M. SCRIVEN, F. SCHULZ, P. GAWEL, L. GROSS, AND H. L. ANDERSON, *An sp-hybridized molecular carbon allotrope, cyclo[18]carbon*, *Science*, 365 (2019), pp. 1299–1301, <https://doi.org/10.1126/science.aay1914>, <https://www.science.org/doi/abs/10.1126/science.aay1914>.
- [15] H. KOCH, A. SCHENKEL, AND P. WITTEWER, *Computer-assisted proofs in analysis and programming in logic: a case study*, *SIAM Review*, 38 (1996), pp. 565–604.
- [16] R. M. KOENIG, H.-R. TIAN, T. L. SEELER, K. R. TEPPER, H. M. FRANKLIN, Z.-C. CHEN, S.-Y. XIE, AND S. STEVENSON, *Fullertubes: Cylindrical carbon with half-fullerene end-caps and tubular graphene belts, their chemical enrichment, crystallography of pristine c_{90} - $d_{5h}(1)$ and c_{100} - $d_{5d}(1)$ fullertubes, and isolation of c_{108} , c_{120} , c_{132} , and c_{156} cages of unknown structures*, *Journal of the American Chemical Society*, 142 (2020), pp. 15614–15623, <https://doi.org/10.1021/jacs.0c08529>, <https://doi.org/10.1021/jacs.0c08529>. PMID: 32830484.
- [17] R. KRAWCZYK, *Newton-algorithmen zur bestimmung von nullstellen mit fehlerschranken*, *Computing (Arch. Elektron. Rechnen)*, 4 (1969), pp. 187–201.
- [18] S. LAIR, W. HERNDON, L. MURR, AND S. QUINONES, *End cap nucleation of carbon nanotubes*, *Carbon*, 44 (2006), pp. 447–455, <https://doi.org/https://doi.org/10.1016/j.carbon.2005.08.027>, <https://www.sciencedirect.com/science/article/pii/S000862230500518X>.
- [19] L. LINDSAY AND D. A. BROIDO, *Optimized tersoff and brenner empirical potential parameters for lattice dynamics and phonon thermal transport in carbon nanotubes and graphene*, *Phys. Rev. B*, 81 (2010), p. 205441, <https://doi.org/10.1103/PhysRevB.81.205441>, <https://link.aps.org/doi/10.1103/PhysRevB.81.205441>.
- [20] E. MAININI, H. MURAKAWA, P. PIOVANO, AND U. STEFANELLI, *Carbon-nanotube geometries: Analytical and numerical results*, *Discrete and Continuous Dynamical Systems - S*, 10 (2017), pp. 141–160, <https://doi.org/10.3934/dcdss.2017008>, <https://www.aims sciences.org/article/id/9b97b9c9-d016-4a3e-abfb-6e2159ecd26f>.
- [21] E. MAININI, H. MURAKAWA, P. PIOVANO, AND U. STEFANELLI, *Carbon-nanotube geometries as optimal configurations*, *Multiscale Model. Simul.*, 15 (2017), pp. 1448–1471, <https://doi.org/10.1137/16M1087862>, <http://cvgmt.sns.it/paper/3131/>. piprints preprint.
- [22] M. MEYYAPPAN, *Carbon Nanotubes: Science and Applications*, CRC Press, Boca Raton, FL, 2004.
- [23] R. E. MOORE, *Interval analysis*, Prentice-Hall Inc., Englewood Cliffs, N.J., 1966.
- [24] P. M. MORSE, *Diatomic molecules according to the wave mechanics. ii. vibrational levels*, *Physical Review*, 34 (1929), pp. 57–64, <https://doi.org/10.1103/PhysRev.34.57>.
- [25] F. MUÑOZ-ALMARAZ, E. FREIRE, J. GALÁN, E. DOEDEL, AND A. VANDERBAUWHEDE, *Continuation of periodic orbits in conservative and hamiltonian systems*, *Physica D: Nonlinear Phenomena*, 181 (2003), pp. 1–38, [https://doi.org/https://doi.org/10.1016/S0167-2789\(03\)00097-6](https://doi.org/https://doi.org/10.1016/S0167-2789(03)00097-6), <https://www.sciencedirect.com/science/article/pii/S0167278903000976>.
- [26] M. T. NAKAO, M. PLUM, AND Y. WATANABE, *Numerical Verification Methods and Computer-Assisted Proofs for Partial Differential Equations*, vol. 53 of Springer Series in Computational Mathematics, Springer, Singapore, 2019.
- [27] D. G. PETTIFOR AND I. I. OLEINIK, *Analytic bond-order potentials beyond tersoff-brenner. i. theory*, *Physical Review B*, 59 (1999), pp. 8487–8499, <https://doi.org/10.1103/PhysRevB.59.8487>.

- [28] P. ROWE, V. L. DERINGER, P. GASPAROTTO, G. CSÁNYI, AND A. MICHAELIDES, *An accurate and transferable machine learning potential for carbon*, The Journal of Chemical Physics, 153 (2020), p. 034702, <https://doi.org/10.1063/5.0005084>, <https://doi.org/10.1063/5.0005084>.
- [29] S. M. RUMP, *INTLAB - INTerval LABoratory*, Hamburg University of Technology, 1999. <https://www.ti3.tuhh.de/rump/intlab/>.
- [30] S. M. RUMP, *Computational error bounds for multiple or nearly multiple eigenvalues*, Linear Algebra and its Applications, 324 (2001), pp. 209–226, [https://doi.org/10.1016/S0024-3795\(00\)00279-2](https://doi.org/10.1016/S0024-3795(00)00279-2), <https://www.sciencedirect.com/science/article/pii/S0024379500002792>.
- [31] S. M. RUMP, *Verification of positive definiteness*, BIT Numerical Mathematics, 46 (2006), pp. 433–452, <https://doi.org/10.1007/s10543-006-0056-1>, <https://doi.org/10.1007/s10543-006-0056-1>.
- [32] R. SAITO, G. DRESSSELHAUS, AND M. S. DRESSSELHAUS, *Physical Properties of Carbon Nanotubes*, Imperial College Press, 1998, <https://doi.org/10.1142/p080>, <https://www.worldscientific.com/doi/abs/10.1142/p080>.
- [33] D. P. SANDERS AND L. BENET, *Intervalarithmic.jl*, 2014, <https://doi.org/10.5281/zenodo.3336308>, <https://github.com/JuliaIntervals/IntervalArithmetic.jl>.
- [34] B. SCHRIEF, *Variationelle analysis von carbonnanoröhren und störungen von ihnen*, master’s thesis, University of Münster, Münster, Germany, November 2022, https://www.uni-muenster.de/imperia/md/content/amm/masterarbeit_benjaminschrief.pdf.
- [35] S. STEVENSON AND H. C. DORN, *Fullertubes: A 30-year story of prediction, experimental validation, and applications for a long-missing family of soluble carbon molecules*, Accounts of Chemical Research, 57 (2024), pp. 2154–2165, <https://doi.org/10.1021/acs.accounts.4c00302>, <https://doi.org/10.1021/acs.accounts.4c00302>. PMID: 39042832.
- [36] J. TERSOFF, *Empirical interatomic potential for carbon, with applications to amorphous carbon*, Phys. Rev. Lett., 61 (1988), pp. 2879–2882, <https://doi.org/10.1103/PhysRevLett.61.2879>, <https://link.aps.org/doi/10.1103/PhysRevLett.61.2879>.
- [37] J. TERSOFF, *New empirical approach for the structure and energy of covalent systems*, Phys. Rev. B, 37 (1988), pp. 6991–7000, <https://doi.org/10.1103/PhysRevB.37.6991>, <https://link.aps.org/doi/10.1103/PhysRevB.37.6991>.
- [38] W. TUCKER, *Validated Numerics*, Princeton University Press, Princeton, NJ, 2011. A short introduction to rigorous computations.
- [39] J. B. VAN DEN BERG AND J.-P. LESSARD, *Rigorous numerics in dynamics*, Notices of the American Mathematical Society, 62 (2015), pp. 1057–1061.
- [40] D. WALES, *Energy Landscapes: Applications to Clusters, Biomolecules and Glasses*, Cambridge Molecular Science, Cambridge University Press, 2004.
- [41] S. J. WEINER, P. A. KOLLMAN, D. T. NGUYEN, AND D. A. CASE, *An all atom force field for simulations of proteins and nucleic acids*, Journal of Computational Chemistry, 7 (1986), pp. 230–252, <https://doi.org/https://doi.org/10.1002/jcc.540070216>, <https://onlinelibrary.wiley.com/doi/abs/10.1002/jcc.540070216>.
- [42] W. C. WITT, C. VAN DER OORD, E. GELŽINYTĚ, T. JÄRVINEN, A. ROSS, J. P. DARBY, C. H. HO, W. J. BALDWIN, M. SACHS, J. KERMODE, N. BERNSTEIN, G. CSÁNYI, AND C. ORTNER, *Acepotentials.jl: A julia implementation of the atomic cluster expansion*, The Journal of Chemical Physics, 159 (2023), p. 164101, <https://doi.org/10.1063/5.0158783>, <https://doi.org/10.1063/5.0158783>.